Dispersion relations for the dust-acoustic wave under experimental conditions

W. D. Suranga Ruhunusiri[a] and J. Goree
Department of Physics and Astronomy, The University of Iowa, Iowa City, Iowa 52242, USA

(Received 4 March 2014; accepted 10 May 2014; published online 30 May 2014)

The dust acoustic wave dispersion relation is tested to quantify its sensitivity to many physical processes that are important in laboratory dusty plasmas. It is found that inverse Landau damping and ion-neutral collisions contribute about equally to the growth rate ω_i, pointing to the advantage of using a kinetic model for the instability. The growth rate ω_i increases the most with an increase of dust number density, followed by an increase in ion-drift speed. The quantities that cause ω_i to decrease the most when they are increased are the dust-neutral collision rate followed by the ion-neutral collision rate, ion collection current onto dust particles, and the ion thermal speed. In general, ω_i is affected more than ω_r by the choice of processes that are included. Strong Coulomb-coupling effects can be included in a compressibility term. The susceptibilities derived here can be combined in various ways in a dispersion relation to account for different combinations of physical processes. © *2014 AIP Publishing LLC*. [http://dx.doi.org/10.1063/1.4879816]

I. INTRODUCTION

A dusty plasma is a mixture of highly charged solid particles, electrons, ions, and neutral gas atoms.[1–9] When a dusty plasma is perturbed, it can sustain a dust acoustic wave (DAW), which is an electrostatic compressional wave that is analogous to an ion acoustic wave.[10] DAW experiments have been performed in both the laboratory[11–46] and under microgravity[47–51] conditions. Inertia for the DAW is provided by the heaviest species, the dust. The restoring force for the DAW is mainly the electric force arising from charge separation of all three charged species, dust, electrons, and ions, as they are compressed and rarefacted. In this wave, the dust particles behave differently from electrons and ions in several ways: they have a much larger inertia, a large cross section for collisions with gas atoms, a charge that fluctuates,[52] and a charge that is large enough to have strong-coupling effects.[53–55]

Our first goal is to assess which physical processes are important for a DAW under experimental conditions. We will rank these processes based on their importance. Our second goal is to weigh the comparative advantages of a kinetic vs. hydrodynamic description of ions. This is needed because most authors use only one of these descriptions, without justifying the choice based on an assessment of its accuracy. We provide that assessment in this paper. Our third goal is to quantify how much the dispersion relation is affected by ion collection current onto dust particles. Our final goal is to formulate a way to incorporate strong-coupling effects using a compressibility parameter for dust, as a measure of the equation of state, and to determine how the sign and magnitude of this parameter affect the dispersion relation.

To meet these goals, we include more physical processes than is commonly done. The processes we include are:

- charge separation
- dust inertia
- ion drift
- ion-neutral collisions
- dust-neutral collisions
- dust compressibility
- finite temperature effects for electron and ions
- ion collection (depletion) onto dust
- dust-charge fluctuations
- inverse Landau damping (ILD) for ions.

We devise a method of testing and ranking the importance of processes. We calculate exponents for the percentage variations of ω_r and ω_i with respect to a parameter that quantifies these processes; a larger exponent indicates a greater effect of this process on the dispersion relation.

This paper begins with a review of the previous DAW literature, emphasizing the methodology of derivations and the expressions for susceptibilities in Secs. II and III, respectively. We derive new susceptibilities for ions, dust, and the dust charge fluctuation in Sec. III, which incorporate more physical processes. We use these expressions in Sec. IV to derive three new dispersion relations. In Sec. V, we present results corresponding to our four goals: ranking the various physical processes according to how much they affect the dispersion relation, assessing the advantage of a kinetic vs. hydrodynamic description of ions, quantifying the change in the dispersion relation due to ion collection by the dust particles, and describing how the sign and magnitude of the compressibility affect the dispersion relation. For the calculations in Secs. IV and V, we assume typical experimental conditions, in particular, the parameters of the DAW experiment of Flanagan and Goree[38] (denoted henceforth as FG). We review this experiment in Appendix A.

II. HOW PHYSICAL PROCESSES ARE INCLUDED IN A DISPERSION RELATION

Two approaches for deriving dispersion relations in a dusty plasma are the lattice wave and hydrodynamic approaches.

[a]Electronic mail: suranga-ruhunusiri@uiowa.edu

In the lattice wave approach, all the physics of electrons and ions are incorporated in a screening length for the interaction of point-like dust particles, and the equation of motion of the dust particles is solved to determine the mode frequencies.[56–59] This lattice wave approach is useful mainly for strongly coupled dusty plasmas in a crystalline state. It predicts longitudinal and transverse waves, but neither of these waves is the same as a DAW; a DAW involves charge separation among the charged species, and the reduced treatment of electrons and ions in the lattice approach does not allow an accounting for this charge separation.

In the hydrodynamic approach, which we use, the fluctuating densities are treated separately for three components: electrons, ions, and dust. The linearized fluctuating densities $\tilde{n}_j$ for each species j are related to the linearized wave potential fluctuations $\tilde{\phi}$ by the susceptibility

$$\chi_j = -\frac{Q_j \tilde{n}_j}{\varepsilon_0 k^2 \tilde{\phi}}. \tag{1}$$

Since the charge on a dust particle can fluctuate,[4,52] one can define a susceptibility χ_{qd}, which relates the linearized fluctuating dust charge $\tilde{Q}_d$ to the linearized wave potential fluctuation $\tilde{\phi}$. This susceptibility can be written as

$$\chi_{qd} = -\frac{\tilde{Q}_d n_d}{\varepsilon_0 k^2 \tilde{\phi}}. \tag{2}$$

To derive a dispersion relation, Eqs. (1) and (2) are combined in the linearized and Fourier transformed Poisson equation, $\epsilon_0 k^2 \tilde{\phi} = \tilde{n}_i Q_i + \tilde{n}_e Q_e + \tilde{n}_d Q_d + n_d \tilde{Q}_d$, yielding

$$\varepsilon(k,\omega) = 1 + \chi_e + \chi_i + \chi_d + \chi_{qd}. \tag{3}$$

Here, k is the wave number, while χ_e, χ_i, and χ_d are the linear susceptibilities for electrons, ions, and dust.

The first DAW dispersion relation was derived by Rao *et al.*[10] Essentially, they solved Eq. (3), omitting χ_{qd}, using separate hydrodynamic descriptions of electrons, ions, and a continuum description of cold dust. The dispersion relation of Rao *et al.*[10] is not suitable for laboratory experiments because it does not take into account effects that are generally present in experiments: drifting ions, frictional gas drag on ions and dust, strong-coupling effects for the dust, and depletion of electrons and ions onto the dust. Some of these effects were included in varying combinations by other authors.[52,60–77] Among them, D'Angelo *et al.*[60] added drifting ions and gas friction acting upon ions and dust, but they did not include dust-charge fluctuation. Melandsø *et al.*[52] added dust-charge fluctuation to the Rao derivation, but they did not include ion drift or gas friction acting on ions and dust.

Depletion of electrons and ions from the plasma,[78–80] due to collection onto the dust, can be a significant factor in experimental plasmas if the cloud of dust particles fills a three-dimensional volume. In a wave, this depletion is enhanced when the cloud is locally compressed. Melandsø *et al.*[52] took this process into account in a theory intended for planetary rings, but without other processes that are significant in experimental conditions such as dust-neutral collisions.

Strong-coupling effects arise due to the discreteness of particles. Discrete particles cause microscopic variations in the electric field. These microscopic effects are most severe if a particle's charge is large, which is the case for dust particles. For this reason, dust particles under experimental conditions tend to be strongly coupled, so that they act collectively like atoms in a liquid or solid.[81,82] Electrons and ions, on the other hand, remain weakly coupled, so that they have collective properties more like those of a gas.

We can identify three approaches that have been taken in the literature to account for strong coupling of dust. Rosenberg and Kalman[64] used a quasi-localized charge approximation for dust to derive the longitudinal component of a dynamical matrix, and they included this in χ_d. Kaw and Sen[65] approximated χ_d as that of a one-component plasma (OCP), as derived by Ichimaru *et al.*[83] Murillo[66] derived the dust susceptibility taking into account strong-coupling effects by using a static local field correction parameter.

One of our goals in this paper is to formulate a hydrodynamic description of strong coupling in terms of a compressibility β. In general, the compressibility of a substance is a measure of the fractional change in its volume divided by the change in pressure. We add a compressibility term, which can be adjusted to account for either strong or weak coupling among dust particles, in the dust equation of motion when we derive a dust susceptibility.

All of the dispersion relations that we discussed above are for waves with small amplitude, i.e., linear waves. The wave amplitude in DAW experiments can be linear[38,40] or nonlinear,[39,40,43,49,50] although experimenters have often found that even under nonlinear conditions the wavelength is predicted reasonably by a linearized dispersion relation.[17]

III. SUSCEPTIBILITY DERIVATION

Here, we present expressions for ion, electron, and dust susceptibilities that include various combinations of physical processes. Readers may use the expressions we list below in any combination desired, to include the physical processes that are deemed to be important.

A. Ion susceptibility

We present five expressions for χ_i, each with a different combination of ion processes. The first four expressions were first reported by other authors, while the last one is developed here. The ion processes that we consider are ion drift, ion-neutral collisions, finite ion-temperature effects, and ion losses by collection onto dust particles.

Either a Vlasov or a hydrodynamic description can be used to describe ions. Other authors have generally chosen one or the other, without justification. An advantage of the Vlasov description is that it is kinetic, so that it includes two effects that are important for the instability: ILD and ion-neutral collisions. Only the latter is included in the hydrodynamic description. However, the hydrodynamic description has its own advantage: it can easily be adapted to account for ion currents collected on the dust particles. One of the goals

of this paper is to weigh the comparative advantages of these two descriptions, for typical experimental conditions; we do this in Sec. V.

1. Vlasov kinetic description

A kinetic Vlasov description for ions is[63]

$$\chi_i = \frac{1}{k^2\lambda_{Di}^2}\frac{1+\xi_i Z(\xi_i)}{[1+(i\nu_{in}/\sqrt{2}kV_{Ti})Z(\xi_i)]}. \tag{4}$$

This assumes an ion-neutral collision rate ν_{in} and a Maxwellian ion distribution centered at an ion drift speed U_0. Here, $\xi_i = (\omega - kU_0 + i\nu_{in})/\sqrt{2}kV_{Ti}$, $V_{Ti} = \sqrt{k_BT_i/m_i}$, and $Z(\xi_i)$ is the plasma dispersion function.[84] The imaginary part of Eq. (4) would correspond to unstable wave growth.

2. Hydrodynamic descriptions

Here, we present four hydrodynamic descriptions with different physical processes.

The first and simplest hydrodynamic description of ions assumes a Boltzmann response $n_i = n_{i0}\exp(-e\phi/k_BT_i)$. The susceptibility is[10]

$$\chi_i = \frac{1}{k^2\lambda_{Di}^2}, \tag{5}$$

where λ_{Di} is the ion Debye length. Equation (5) assumes that the ions are inertialess, and it neglects many processes for ions important for laboratory experiments. We will next add several processes, one at a time.

In our second hydrodynamic description, we add ion drift, which is one of two required elements for destabilization of the wave in a hydrodynamic approach. Assuming a drift speed U_0, the ion fluid velocity is written as $u_i = U_0 + \tilde{u}_i$, which we use in the ion fluid equations

$$\frac{\partial n_i}{\partial t} + \frac{\partial}{\partial z}n_iu_i = 0 \tag{6}$$

and

$$\frac{d}{dt}u_i = -\frac{e}{m_i}\frac{\partial}{\partial z}\phi - \frac{k_BT_i}{n_im_i}\frac{\partial n_i}{\partial z}. \tag{7}$$

After linearizing, Fourier transforming, and combining Eqs. (6) and (7) into Eq. (1), we obtain

$$\chi_i = \frac{\omega_{pi}^2}{V_{Ti}^2k^2 - (kU_0-\omega)^2}. \tag{8}$$

Here, n_i is the ion number density, while m_i, T_i, and ω_{pi} are the ion mass, ion kinetic temperature, and ion plasma frequency. The ion momentum equation, Eq. (7), has terms on its right hand side for the macroscopic electric force (due to charge separation) and the ion pressure. Since the ions are weakly coupled, an ideal gas equation of state is used for the ion pressure.

Our third description adds the other required element for destabilization of the wave in a hydrodynamic approach: ion-neutral collisions. We rewrite the ion momentum equation, Eq. (7), as

$$\frac{d}{dt}u_i = -\frac{e}{m_i}\frac{\partial}{\partial z}\phi - \frac{k_BT_i}{n_im_i}\frac{\partial n_i}{\partial z} - \nu_{in}u_i. \tag{9}$$

Combining this with Eq. (6) yields

$$\chi_i = \frac{\omega_{pi}^2}{V_{Ti}^2k^2 - (kU_0-\omega)^2 + i\nu_{in}(kU_0-\omega)}. \tag{10}$$

The three hydrodynamic descriptions listed above, Eqs. (5), (8), and (10), have previously appeared in the literature. Equation (10), in particular, was used earlier by FG[38] for the limit $U_0 \gg \omega/k$.

Our fourth hydrodynamic description adds one more process: ion losses due to the collection of ions on the dust particles. To do this, we add a term to the ion continuity equation

$$\frac{\partial n_i}{\partial t} + \frac{\partial}{\partial z}n_iu_i = -n_dI_i/e. \tag{11}$$

The last term is the ion loss rate onto the dust, which is proportional to both the dust number density n_d and the ion current onto dust I_i. In a wave, the ion current I_i will be modulated and this will modify the modulation of n_i and thereby affect χ_i. One can in principal use any model for this ion current. In this paper, we will use two such models. First, the orbital-motion limited (OML) ion current is[85]

$$I_i = \pi a^2 n_i u_i e\left(1 - \frac{2e\phi_s}{m_iu_i^2}\right), \tag{12}$$

and this takes into account ion drift, but not ion-neutral collisions. Here, $\phi_s = Q_d/4\pi\varepsilon_0 a$ is the dust particle surface potential for a particle of radius a. Second, the Lampe ion current,[86] which accounts for ion-neutral collisions but not ion drift, is

$$I_i = \sqrt{8\pi}a^2n_iV_{Ti}\left[1 + z\tau + \left(R_0^3/a^2l_i\right)\right]. \tag{13}$$

The symbols inside the square brackets of Eq. (13) are defined in Khrapak *et al.*[87]

For the experimental conditions of FG,[38] the Lampe ion current (without ion drift) is approximately double the OML ion current (without ion-neutral collisions). Ideally, a third ion current model is needed that accounts for *both* ion drift and ion-neutral collisions, but we are not aware of any analytical model that does this.

After the usual linearization and Fourier transformation, we combine Eqs. (9), (11), and (12) into Eq. (1). This yields (see the supplementary material[88] for the derivation)

$$\chi_i = \frac{\Omega_\phi}{k^2\lambda_{Di}^2(\Omega_n - i\omega)}. \tag{14}$$

Here, Ω_n and Ω_ϕ are quantities, which have dimensions of inverse time, and they depend only on equilibrium parameters such as n_{i0} and U_0. Expressions for Ω_n and Ω_ϕ are rather

lengthy; they are presented in Appendix B along with an adjustable parameter that allows their use with the Lampe model or any other model of ion current.

B. Electron susceptibility

Electrons in a dusty plasma, like ions, are generally weakly coupled, so that they can be described either hydrodynamically, or with a kinetic Vlasov description.

Neglecting inertia, electrons are described by the Boltzmann response, $n_e = n_{e0}\exp(e\phi/k_BT_e)$, as in Rao *et al.*[10] The susceptibility is then

$$\chi_e = \frac{1}{k^2\lambda_{De}^2}, \tag{15}$$

where λ_{De} is the electron Debye length.

Alternatively, the Vlasov description of electrons[63] including electron-neutral collisions is

$$\chi_e = \frac{1}{k^2\lambda_{De}^2}\frac{1+\xi_e Z(\xi_e)}{[1+(i\nu_{en}/\sqrt{2}kV_{Te})Z(\xi_e)]}. \tag{16}$$

Such a kinetic description retains the effects of electron Landau damping, but this is usually unnecessary as the phase velocity of the DAW is usually very slow compared to the electron thermal velocity. For this reason, we only use Eq. (15) in our derivation of DAW dispersion relations.

C. Dust susceptibility

The dust particles experience many processes that affect their motion, and these enter into the dust susceptibility χ_d. Most significantly, the dust particles provide inertia to the wave and they participate in the charge separation that is responsible for wave's electric field. Additionally, dust-neutral collisions introduce wave damping. As the dust is compressed and rarefied, the dust equation of state comes into play, and this is described by the compressibility, which must be chosen differently according to whether the dust is weakly or strongly coupled.

We do not use a Vlasov kinetic description for the dust particles in a dusty plasma. Such a description is not appropriate when collisional nearest neighbor interactions of dust particles are strong, as is often the case under experimental conditions. Thus, we choose a hydrodynamic description for dust, which we can adapt to include strong-coupling effects.

We generalize the hydrodynamic approach of FG[38] by including the dust compressibility β to the dust fluid equations. To derive the dust susceptibility, the dust fluid equations

$$\frac{\partial n_d}{\partial t} + \frac{\partial}{\partial z}n_d u_d = 0 \tag{17}$$

and

$$\frac{d}{dt}u_d = -\frac{Q_d}{m_d}\frac{\partial}{\partial z}\phi - \frac{1}{\beta n_d^2 m_d}\frac{\partial n_d}{\partial z} \tag{18}$$

are linearized, Fourier transformed, and combined into Eq. (1) to yield

$$\chi_d = \frac{\omega_{pd}^2}{k^2(\beta n_d m_d)^{-1} - \omega^2}. \tag{19}$$

Here, m_d and u_d are the dust particle mass and dust fluid speed. The two terms on the right hand side of the dust momentum equation, Eq. (18), are the wave's macroscopic electric force (due to charge separation) and the dust pressure gradient terms.

We can further generalize the dust susceptibility to incorporate dust-neutral collisions. Accordingly, we introduce the dust-neutral damping term with a rate ν_{dn} to the right hand side of Eq. (18), yielding

$$\frac{d}{dt}u_d = -\frac{Q_d}{m_d}\frac{\partial}{\partial z}\phi - \frac{1}{\beta n_d^2 m_d}\frac{\partial n_d}{\partial z} - \nu_{dn}u_d. \tag{20}$$

The dust susceptibility is then

$$\chi_d = \frac{\omega_{pd}^2}{k^2(\beta n_d m_d)^{-1} - \omega(\omega + i\nu_{dn})}. \tag{21}$$

The compressibility β deserves discussion because this parameter is the only one in our dispersion relation that can account for strong-coupling effects for the dust. In the case of weak coupling, with no microscopic electric forces between individual dust particles, we would have an ideal gas equation of state for the dust. The compressibility then has the positive value $\beta = 1/n_d k_B T_d$, and Eq. (21) becomes

$$\chi_d = \frac{\omega_{pd}^2}{k^2 V_{Td}^2 - \omega(\omega + i\nu_{dn})}, \tag{22}$$

where $V_{Td} = \sqrt{k_B T_d/m_d}$. For strong coupling, the compressibility arises from microscopic variations in the electric field due to the discreteness of particles. The compressibility can be a complex number due to viscoelastic effects, and our expressions allow for this possibility, although later we will assume β is real and does not vary with ω or k. The effects of β on the DAW dispersion relation will be quantified in Sec. V D.

D. Susceptibility due to dust-charge fluctuation

Dust particles charge by collecting electrons and ions. These collection currents can fluctuate at the wave's frequency so that the dust charge Q_d will fluctuate as well.[52] Due to this dust-charge fluctuation, some authors have included a fourth susceptibility, Eq. (2), into their derivation of the DAW dispersion relations. All the other susceptibilities we have considered are based on Eq. (1) due to fluctuations of a number density.

Here, we derive an expression for χ_{qd} by generalizing the hydrodynamic approach of Melandsø *et al.*[52] by including four more processes: ion drift, ion-neutral collisions, dust-neutral collisions, and strong-coupling effects for dust. We start with the dust charging equation

$$\frac{\partial Q_d}{\partial t} = I_e + I_i, \tag{23}$$

where I_e and I_i are the electron and ion currents, respectively. In principal, one can use any model for these currents. For

consistency, we again use the OML current model,[85] Eq. (12) for ions and

$$I_e = -4\pi a^2 n_e e \sqrt{\frac{k_B T_e}{2\pi m_e}} \exp\left(\frac{e\phi_s}{k_B T_e}\right) \tag{24}$$

for electrons.

To obtain an expression for this susceptibility, we linearize, Fourier transform, and combine Eqs. (12), (23), and (24) into Eq. (2). This yields (see the supplementary material[88] for the derivation)

$$\chi_{qd} = -\frac{4\pi a n_{d0} \Omega_{V0}}{k^2(\Omega_{\phi s} - i\omega)}. \tag{25}$$

Here, $\Omega_{\phi s}$ and Ω_{V0} are quantities having the dimensions of inverse time and they are functions of equilibrium quantities like n_{i0} and n_{e0}. Expressions for $\Omega_{\phi s}$ and Ω_{V0} are rather lengthy and they are presented in Appendix B. For use with other ion current models, these expressions contain an adjustable parameter.

IV. MODELS FOR DAW DISPERSION RELATIONS

We now derive three new dispersion relations that include a combination of physical effects from the list in Sec. I. We do this by combining various susceptibilities from Sec. III into Eq. (3). The sensitivity of the dispersion relations to these effects is quantified in Sec. V.

A. Baseline hydrodynamic model

We start with a baseline dispersion relation that includes minimal effects appropriate for experimental plasmas: charge separation, dust inertia, ion drift, ion-neutral collisions, dust-neutral collisions, an adjustable compressibility, and finite temperature effects for electrons and ions. These are the first seven effects from the list in Sec. I. Our other two dispersion relations will be generalizations of this baseline dispersion relation, which in turn is a generalization of the dispersion relation of FG.[38]

We use a dust susceptibility that includes a compressibility. The compressibility can be selected either for a weak-coupling case using $\beta = 1/n_d k_B T_d$ or a strong-coupling case using another value.

We combine Eqs. (21), (15), and (10) for χ_d, χ_e, and χ_i, respectively, in Eq. (3). For now, we omit χ_{qd}, i.e., we neglect the dust-charge fluctuation at the wave's frequency. The resulting baseline dispersion relation is

$$\varepsilon(k,\omega) = \left\{1 + \frac{1}{k^2\lambda_{De}^2} + \frac{\omega_{pi}^2}{V_{Ti}^2 k^2 - (kU_0 - \omega)^2 + i\nu_{in}(kU_0 - \omega)} + \frac{\omega_{pd}^2}{k^2(\beta n_d m_d)^{-1} - \omega(\omega + i\nu_{dn})}\right\} = 0. \tag{26}$$

It is typically the case that $U_0/(\omega/k) \gg 1$; for example, in the experiment of FG,[38] this ratio is 9500. In this limit, Eq. (26) has an analytical solution

$$\omega(k) = \omega_{pd}\left[k\lambda_{De}\sqrt{\frac{1}{1 + k^2\lambda_{De}^2\alpha} + \frac{1}{\beta n_d m_d \omega_{pd}^2 \lambda_{De}^2} - \frac{\nu_{dn}^2}{4\omega_{pd}^2 k^2 \lambda_{De}^2}} - i\frac{\nu_{dn}}{2\omega_{pd}}\right]. \tag{27}$$

In Eq. (27), $\alpha \equiv 1 + \omega_{pi}^2/\left[\left(V_{Ti}^2 - U_0^2\right)k^2 + i\nu_{in}U_0 k\right]$ is a dimensionless complex quantity, which has a value of about $0.8 - 1.7i$ for the typical experimental conditions of FG.[38]

The wave frequency and growth rate are the real and imaginary parts of Eq. (27), respectively. We plot them in Fig. 1, assuming real k, using the experimental parameters of FG.[38]

In this baseline model, ion-neutral collisions destabilize the wave while the dust-neutral collisions provide wave damping. This can be seen in Fig. 2, which is a plot of the growth rate ω_i vs. ion-neutral collision rate ν_{in} based on Eq. (27). The instability occurs only for $\nu_{in} > 2.5 \times 10^6\,\mathrm{s}^{-1}$ for the conditions of FG.[38]

B. Hydrodynamic model with more processes

Next, we add two additional processes to our baseline model: ion collection onto dust and dust-charge fluctuations.

Combining Eqs. (25), (21), (15), and (14) for χ_{qd}, χ_d, χ_e, and χ_i, respectively, in Eq. (3) yields

$$\varepsilon(k,\omega) = \left\{1 + \frac{1}{k^2\lambda_{De}^2} + \frac{1}{k^2\lambda_{Di}^2}\frac{\Omega_\phi}{(\Omega_n - i\omega)} + \frac{\omega_{pd}^2}{k^2(\beta n_d m_d)^{-1} - \omega(\omega + i\nu_{dn})} - \frac{4\pi a n_d}{k^2}\frac{\Omega_{V0}}{(\Omega_{\phi s} - i\omega)}\right\} = 0. \tag{28}$$

In this dispersion relation, the quantities Ω_ϕ, Ω_n, $\Omega_{\phi s}$, and Ω_{V0} all have dimensions of inverse time as presented in Appendix B. Typical values of these four quantities for the experimental parameters of FG[38] are: $\Omega_\phi = (7.1 - 3.2i) \times 10^5\,\mathrm{s}^{-1}$, $\Omega_n = (0.7 + 4.2i) \times 10^6\,\mathrm{s}^{-1}$, $\Omega_{\phi s} = 4.7 \times 10^5\,\mathrm{s}^{-1}$, and $\Omega_{V0} = -(0.3 + 2.7i) \times 10^6\ \mathrm{s}^{-1}$. These values are for the OML ion current model, which we also assume in the remainder of this paper except in Sec. V C, where we examine the sensitivity of the dispersion relations to the choice of ion current model.

In this hydrodynamic model, as with our baseline model, the mechanism that destabilizes the DAW is

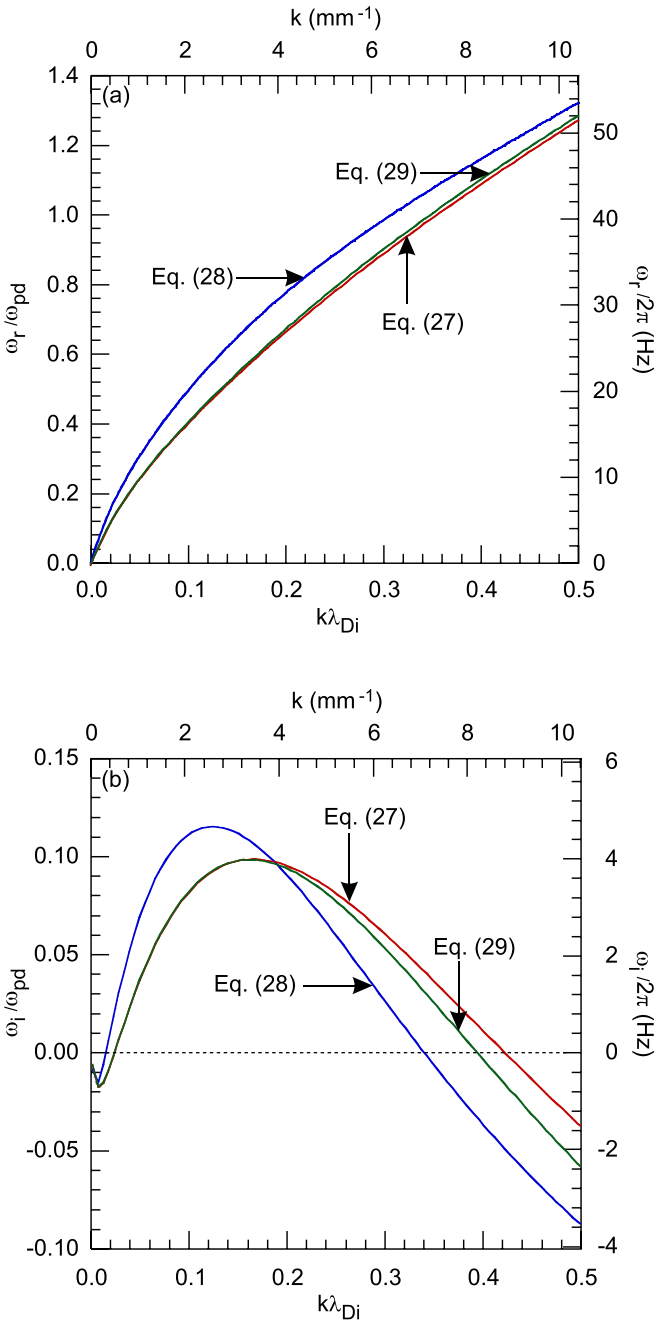

FIG. 1. Real frequency ω_r (a) and imaginary frequency ω_i (b) as a function of wavenumber k for three dispersion relation models derived in Sec. IV. These models are: the baseline hydrodynamic model Eq. (27), hydrodynamic model with more processes Eq. (28), and hybrid hydrodynamic-kinetic model Eq. (29), respectively. We use the experimental conditions of FG[38] as input parameters for these models. All the three models yield a maximum growth rate near $4\,\mathrm{mm}^{-1}$, which is the experimentally observed wave number in FG.[38]

ion-neutral collisionality. However, unlike the baseline model, Eqs. (26) and (27), in Eq. (28), wave damping is provided not only by dust-neutral collisions but also by dust-charge fluctuations.

Equation (28) requires a numerical solution. We plot this solution in Fig. 1.

Comparing the curves in Fig. 1, we find that including the two additional processes, ion collection on dust particles and dust-charge fluctuation, has an effect up to 40% in the dispersion relation. This is seen in Figs. 1(a) and 1(b), where

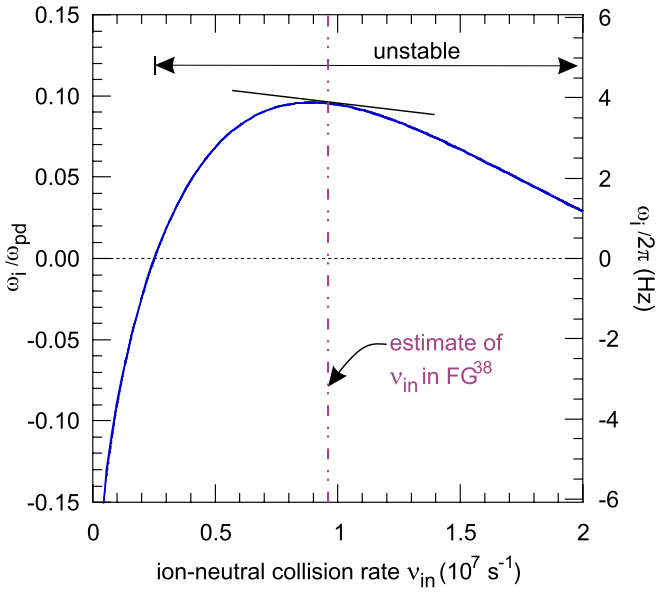

FIG. 2. Sensitivity of the growth rate ω_i to the ion-neutral collision rate ν_{in}. The curve is obtained by solving Eq. (27), the dispersion relation for the baseline model, for the experimental conditions of FG[38] except that we allow ν_{in} to vary. The wave number is $k = 4\,\mathrm{mm}^{-1}$. A tangent is drawn at the estimate of ν_{in} in FG.

we compare the model that includes these processes to the baseline model, which does not. In particular, both ω_r and ω_i are changed by as much as 40% over a wide range of k.

C. Hybrid hydrodynamic-kinetic model

Next, we include the same effects as in our baseline model, except now for ions we use a kinetic description, which retains the effects of inverse Landau damping.

We use the kinetic susceptibility Eq. (4) for ions with the hydrodynamic susceptibilities Eqs. (15) and (21) for electrons and dust. These are combined in Eq. (3). Here, we omit the susceptibility due to dust-charge fluctuation, i.e., χ_{qd}. The resulting hybrid hydrodynamic-kinetic dispersion relation is

$$\varepsilon(k,\omega) = \left\{ 1 + \frac{1}{k^2\lambda_{De}^2} + \frac{1}{k^2\lambda_{Di}^2}\frac{1+\xi_i Z(\xi_i)}{[1+(i\nu_{in}/\sqrt{2}kV_{Ti})Z(\xi_i)]} + \frac{\omega_{pd}^2}{k^2(\beta n_d m_d)^{-1} - \omega(\omega + i\nu_{dn})} \right\} = 0, \tag{29}$$

which also requires a numerical solution. This solution is plotted in Fig. 1 for the experimental parameters of FG.[38]

As it was for the baseline model, the wave damping is provided by dust-neutral collisions. However, unlike the baseline model, here there are two wave destabilization sources: ion inverse Landau damping and ion-neutral collisions. In Sec. V, we will compare these wave destabilization sources and determine their relative contributions to the instability for typical experimental conditions.

We find that the dispersion relation for this hybrid model yields about the same ω_r and ω_i as for our baseline model. As can be seen in Fig. 1, the percentage difference for ω_r between our baseline and the hybrid models are less than 2% over a wide range of k. However, the difference for ω_i is much larger, with a percentage difference of up to 8%.

V. RESULTS AND DISCUSSION

We present our results organized into four subsections that correspond to our four goals. First, we perform a sensitivity test to quantify how much the real and imaginary parts of the wave frequency change, for a given change in an input parameter (such as the ion-neutral collision rate). Second, we determine whether it is important to use a kinetic treatment for ions (which takes into account inverse Landau damping), or whether a simpler hydrodynamic model for the ions is adequate. Third, we quantify how much the dispersion relation depends on the choice of ion current models (OML vs. Lampe). Finally, we use our formalism of χ_d including a compressibility (which can account for strong coupling) to learn how the dispersion relation depends on the sign and magnitude of the compressibility.

A. Sensitivity to parameters

To determine the sensitivity of the dispersion relation to the physical parameters, we calculate exponents

$$\delta_r = (\Delta\omega_r/\omega_r)/(\Delta F/F) \tag{30}$$

and

$$\delta_i = (\Delta\omega_i/\omega_i)/(\Delta F/F), \tag{31}$$

where F is a parameter such as the ion-drift speed U_0. In this test, we make a 1% change in F and we determine the fractional change in ω_r and ω_i to compute δ_r and δ_i, respectively. As an example, if ω_r is proportional to F, the exponent will be unity and if it is proportional to $\sqrt{F}$ the exponent will be 0.5. When calculating these exponents, we assume the experimentally observed wave number $k = 4\,\mathrm{mm}^{-1}$ of FG.[38]

The results for the exponents of ω_r and ω_i are summarized in Table I for our three dispersion relation models derived in Sec. IV. In Table I, we highlight the exponents >0.4 because these indicate a particularly significant sensitivity.

TABLE I. Exponents δ_r and δ_i computed using Eqs. (30) and (31) for the three dispersion relation models derived in Sec. IV. The first column is the parameter F in Eq. (30). Here, we assume the OML model for I_i with $\gamma = 1$. Exponents greater than 0.40 indicate a particularly high sensitivity as marked here in bold. Note: an entry of 0.00* in this table indicates that the magnitude of the exponent is less than 0.01.

	Hydrodynamic models					
	Baseline model		with more processes		Hybrid hydrodynamic-kinetic model	
F	δ_r	δ_i	δ_r	δ_i	δ_r	δ_i
β	−0.11	**+0.44**	−0.09	+0.34	−0.11	**+0.43**
ν_{dn}	−0.12	**−2.24**	−0.09	**−2.39**	−0.12	**−2.28**
ν_{in}	**+0.47**	−0.16	**+0.42**	**−0.61**	**+0.45**	−0.17
U_0	**+0.48**	**+0.87**	+0.29	**+1.49**	**+0.48**	**+0.80**
V_{Te}	−0.00*	+0.13	+0.12	+0.04	−0.00*	+0.14
V_{Ti}	−0.00*	**−0.42**	−0.00*	**−0.43**	+0.01	**−0.44**
ω_{pe}	+0.00*	−0.13	−0.25	+0.08	+0.00*	−0.14
ω_{pi}	**−0.95**	−0.35	**−0.73**	+0.15	**−0.94**	−0.26
ω_{pd}	**+0.88**	**+4.13**	**+0.87**	**+4.39**	**+0.88**	**+4.16**
I_i			+0.14	**−0.59**		
I_e			−0.12	+0.15		

In general, we find that ω_i is more sensitive to changes in various parameters than is ω_r. For example, in Table I, $|\delta_i|$ can be as large as four, whereas $|\delta_r|$ is never large as unity.

We now rank the parameters that cause the largest changes in the growth rate ω_i. When they are increased, the parameters that cause the largest *positive* change in ω_i are the dust plasma frequency followed by the ion-drift speed. For these parameters, $\delta_i > 0.4$ in Table I. On the other hand, the parameters that cause the largest *negative* change in ω_i when they are increased are the dust-neutral collision rate followed by the ion-neutral collision rate, ion current, and ion thermal speed. All of these have $\delta_i < -0.4$ in Table I.

We also rank the parameters that cause the largest changes in the wave's frequency ω_r. Only two parameters, the dust-plasma frequency followed by the ion neutral collision rate, have a significant positive sensitivity with $\delta_r > 0.4$. Only one parameter, the ion plasma frequency, has a significant negative sensitivity with $\delta_r < -0.4$. This list is shorter than for ω_i because, in general, ω_i is much more sensitive than ω_r to a change in a parameter's value.

An experimenter additionally might wish to know the sensitivity of ω_r and ω_i to experimental parameters such as the macroscopic dc electric field E_{0z} or the ambient gas pressure P. We perform a sensitivity analysis for seven such experimental parameters in Appendix C.

We note a limitation of these rankings based on exponents: they are valid only within a narrow range of parameters that brackets the conditions we assumed. While the conditions of FG[38] that we assumed are representative of many experiments, it would be necessary to recompute these exponents if the conditions differ significantly from those of FG. To illustrate this, we show in Fig. 2 results for growth rate ω_i as a function of the dust neutral collision rate ν_{in}. In Fig. 2, a tangent is drawn at the conditions of FG. The exponent is proportional to the slope of the tangent which varies with ν_{in}.

B. Comparison of the sources of the DAW instability

In Sec. IV, we derived three dispersion relation models for the DAW, and among them only the hybrid hydrodynamic-kinetic model has two sources for the DAW instability: ion-neutral collisions and ILD. Here, we compare the contributions to the instability from these two sources.

To distinguish the instability contributions from the ion-neutral collisions and ILD, we compute the imaginary frequency by numerically solving one of our dispersion relations, Eq. (29), two ways: with an ion-neutral collision rate that has a realistic value for experiments and a zero rate, $\nu_{in} = 0$. We subtract the imaginary frequencies calculated using these two ways to find the contribution due to ion-neutral collisions.

The results in Fig. 3 are presented with different hatching patterns for the two contributions to ω_i. We calculate these for the experimental conditions of FG.[38]

We find that the contributions to the instability from ILD and ion-neutral collisions are of the same order of magnitude. In Fig. 3, both contributions are displayed as positive quantities that offset the negative contribution due to gas damping $-0.26\omega_{pd}$. The gas damping contribution is shown as a solid line at the bottom of the Fig. 3. Although the

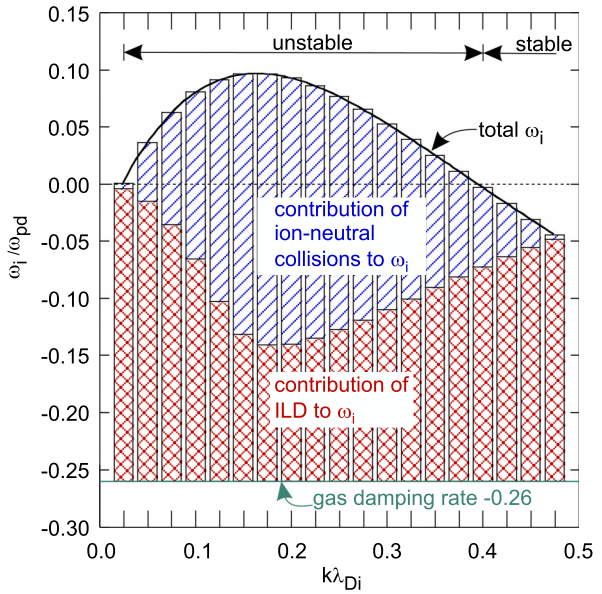

FIG. 3. Contributions of ILD and ion-neutral collisions to the DAW instability for the conditions of FG.[38] The total ω_i (heavy line) and the contributions from ILD (crosshatch pattern) were obtained from Eq. (29) using experimental estimate of ν_{in} in FG[38] and $\nu_{in}=0$, respectively. The difference between the total and ILD contributions is attributed to ion-neutral collisions (single hatch pattern). We find that ILD and ion-neutral collisions contribute about equally to the DAW for these typical experimental conditions.

contributions from ILD and ion-neutral collisions generally vary with k in Fig. 3, as depicted by bars of varying heights, they are generally of the same order of magnitude. For example, at a typical experimental value of $k=4\,\mathrm{mm}^{-1}$ ($k\lambda_{Di}=0.2$ in dimensionless units) as observed in FG,[38] the contribution of ILD is approximately 51% of ion-neutral collisions. We cannot yet, however, make a clear recommendation to use the kinetic model because it neglects ion currents collected by the dust particles, which we will evaluate in Sec. V C.

To yield a positive growth rate from ILD requires a significant population of ions at the wave phase velocity ω_r/k.[89] For the conditions of FG,[38] $\omega_r/k=1.0\times10^{-4}U_0$ and $U_0=1.6V_{Ti}$. For these conditions and for a Maxwellian distribution of ions, the ion population at the wave's phase velocity is 30% of the peak of the distribution, which is sufficient to provide a positive ILD contribution to ω_i (although not enough by itself to overcome the gas damping rate) as depicted in Fig. 3.

It is intriguing that while our baseline hydrodynamic and hybrid hydrodynamic-kinetic models have different sources for the instability, these two models yield roughly the same value for the imaginary part of the frequency, as can be seen in Fig. 1(b). We believe that this equality arises purely by chance for the conditions used. For example, at the much lower gas pressure conditions of an anodic plasma, an instability requires kinetic effects.[25]

C. Sensitivity to ion current model

We find here that ω_i is quite sensitive to the effects of ion current onto the dust particles. The growth rate is significantly suppressed by this ion collection, and this trend has not been noted in the literature, to the best of our knowledge.

In Fig. 4, we compare one of our dispersion relations, Eq. (28), for three cases: I_i is either zero, the OML current, or the Lampe current. The Lampe current is double the OML current for the experimental conditions we consider.

We find that the effect of ions collecting on the dust particles is a reduced growth rate as seen in Fig. 4(b). At $k=4\,\mathrm{mm}^{-1}$, for example, ω_i is reduced by 32% for the OML current as compared to the case for $I_i=0$. It is reduced even more, by 82%, for the Lampe current. The real part of the dispersion relation is also affected, but to a lesser degree than ω_i.

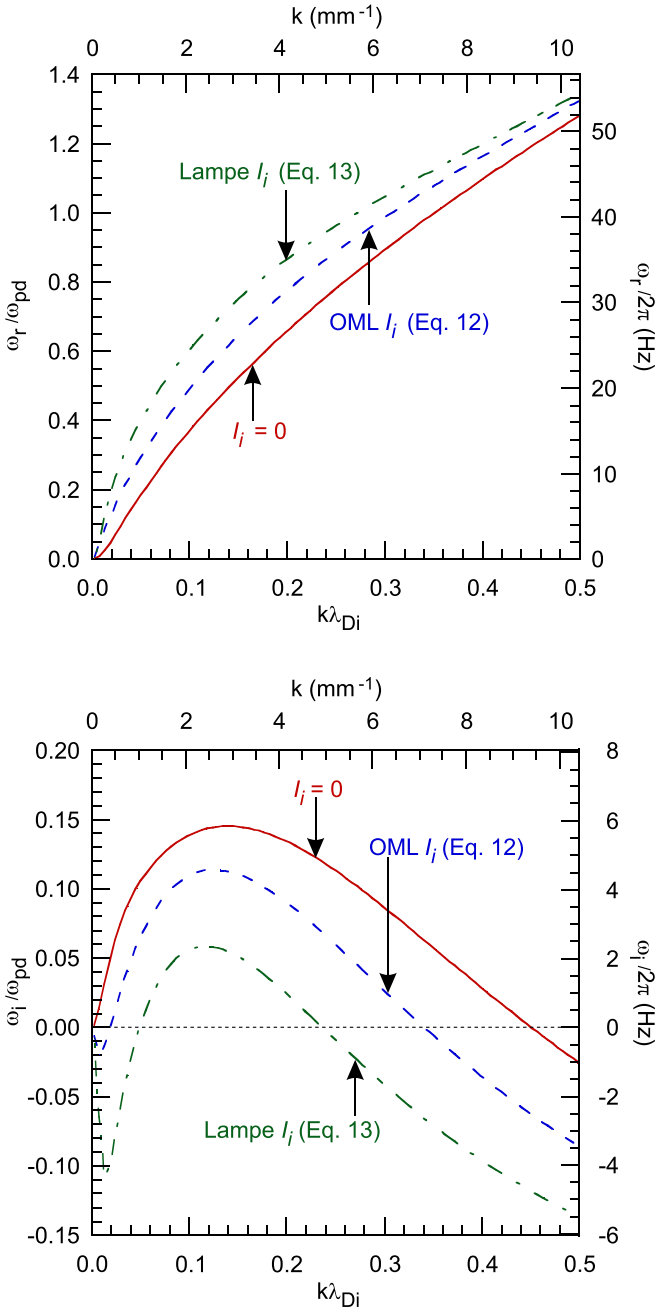

FIG. 4. Real frequency ω_r (a) and imaginary frequency ω_i (b), from Eq. (28), for three different ion currents. For the Lampe current, we use the expression in Appendix B with a parameter γ chosen as the ratio of the ion currents in Eqs. (12) and (13). In particular, for the condition of FG,[38] the Lampe ion current is twice the OML ion current, i.e., $\gamma=2$. The imaginary frequency is affected significantly by the change in the ion current while the real frequency is affected to a lesser degree. These results reveal that the instability is significantly suppressed for enhanced ion currents.

As we mentioned in Sec. III A, the OML ion current, Eq. (12), neglects ion-neutral collisions while the Lampe current, Eq. (13), neglects ion drift. These are both significant processes under experimental conditions. However, we cannot determine, which is more suitable because each model neglects a significant process.

D. Strong coupling effects

The compressibility of a strongly coupled plasma arises from microscopic variations in the electric fields. This compressibility does not generally provide the wave's restoring force; that is done by the macroscopic electric fields arising from charge separation. The role of the compressibility is to somewhat alter that restoring force. In general, a small compressibility would have a large effect on the wave, while a large compressibility would have a little effect; this is because a small compressibility would indicate a significant force for a given change in volume.

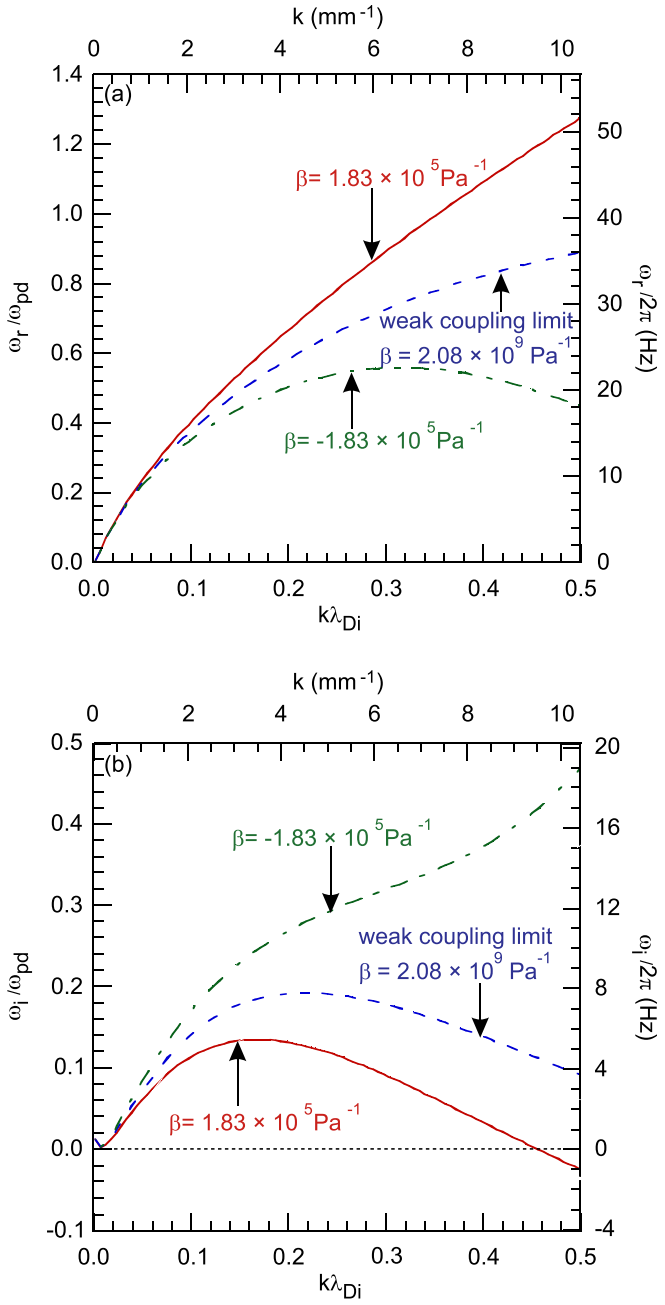

FIG. 5. Real frequency ω_r (a) and imaginary frequency ω_i (b) as a function of wavenumber k from Eq. (27), for three different compressibility values. The three curves in each figure are for a positive compressibility equal to an empirical estimate in FG[38] (solid line), a negative value with the same magnitude as the positive value (dotted-dashed line) and a weak coupling limit value for compressibility (dashed line). We find that the instability is enhanced with a larger ω_i if the compressibility is negative.

In the limit of weak coupling, the compressibility has the ideal gas value $\beta = 1/n_{d0}k_BT_d$. This has such a large value that it will result in little effect on the restoring force. For strong coupling, however, $|\beta|$ can have a much smaller value, thereby have a larger role in altering the wave's restoring force. However, the value of β for a strongly coupled dusty plasma has not been well established, as we will discuss in a future paper. For now, we will adopt a general view, allowing the sign of β to be either positive or negative for strong coupling, when we evaluate the dispersion relation.

We can illustrate how the real and imaginary frequencies are affected by the compressibility. To do this, we solve Eq. (27) for three cases for β: a positive value of $1.83 \times 10^5\,\mathrm{Pa}^{-1}$, which we base on an empirical estimate in FG,[38] a negative value of $-1.83 \times 10^5\,\mathrm{Pa}^{-1}$, and a weak-coupling value of $2.08 \times 10^9\,\mathrm{Pa}^{-1}$. The latter was evaluated as $\beta = 1/n_{d0}k_BT_d$ assuming $n_{d0} = 1.2 \times 10^{10}\,\mathrm{m}^{-3}$ from FG[38] and an estimated value $T_d = 1/40\,\mathrm{eV}$, which is room temperature. The room-temperature assumption for dust is appropriate only for low-amplitude waves, when the dust's random motion is nearly in thermal equilibrium with the neutral gas.

Results plotted in Fig. 5 reveal that compressibility can have a significant effect on the DAW dispersion relation. This is especially so as the wave number k becomes larger, i.e., as the wavelength becomes smaller. The imaginary part is affected more than the real part.

Assuming that strong coupling leads to a *negative* compressibility, we find the trends reported by Rosenberg *et al.*[90] These trends are a smaller ω_r/ω_{pd} and a larger ω_i/ω_{pd} as strong coupling effects are increased. In other words, if all other things including ω_{pd} are held constant, the instability can be enhanced by strong coupling if $\beta < 0$. Alternatively, assuming strong coupling leads to a *positive* compressibility, the trends are reversed: for strongly coupling, the real frequency would be enhanced and the imaginary part would be diminished.

VI. CONCLUSIONS

Including more physical processes than are typically accounted for, we derived new susceptibility expressions for the ions, dust, and dust charge fluctuation. We have also reviewed other susceptibilities that were previously used in the literature. Demonstrating the use of these susceptibilities, we combined them differently to derive three new dispersion relations, which we plotted using the experimental parameters from Flanagan and Goree.[38]

We find that, in general, varying the experimental parameters or selecting different physical processes results in a larger effect on the imaginary part of the dispersion relation than on the real part. This means that for a study of the instability, it is crucial to include the appropriate physical

processes. We performed tests to determine, which processes are important in typical laboratory experiments.

For our first goal, we quantify how sensitive the dispersion relation is to a physical parameter, and the corresponding physical process, by calculating exponents δ_r and δ_i, defined in Eqs. (30) and (31). We judge a parameter to be significant if it alters the frequency enough as judged by $|\delta_r| > 0.4$ or $|\delta_i| > 0.4$. We find that six theoretical parameters affect ω_i substantially; ranking them starting with the largest $|\delta_i|$, for the experimental conditions of FG.[38] These six parameters are

- dust plasma frequency
- dust-neutral collision rate
- ion-drift speed
- ion-neutral collision rate
- ion current
- ion thermal speed.

We also find three experimental parameters that affect ω_r substantially. Starting with the largest $|\delta_r|$, they are

- dust plasma frequency
- ion-plasma frequency
- ion-neutral collision rate.

We find that the DAW instability is significantly suppressed if any physical process leads to a greater collection of ion currents on the dust particles. The real frequency, on the other hand, has little dependence on the ion current. These ion-current effects for the DAW instability will be most important at high dust number densities that are typical of laboratory experiments. This importance of ion currents to laboratory conditions has not been remarked upon in the literature to the best of our knowledge.

We find that the instability contributions from inverse Landau damping and ion-neutral collisions are of the same order. All the other things being the same, it is best to use a kinetic descriptions for ions. However, we are faced with the problem that ion currents, which we also deemed to be important just above, are not easily accounted for in a kinetic model. Thus, there remains a need to derive a more complete expression for χ_i that includes both ILD and ion collection onto dust.

For our final goal, we find that strong coupling can change the growth rate substantially, and it can also make a measurable change in the real frequency as well. We determined this by comparing three cases for the compressibility. Our finding that the dispersion relation is sensitive to the compressibility indicates a need for further studies of compressibility of strongly coupled plasmas to determine its magnitude and sign.

ACKNOWLEDGMENTS

This work was supported by NASA and NSF.

TABLE II. Input parameters for solving the dispersion relation from the DAW experiment of FG.[38] We choose the value of β based on an empirical estimate of a sound speed in FG.

Parameter	Value
n_{i0}	$6.0 \times 10^{14}\,\mathrm{m}^{-3}$
n_{e0}	$2.0 \times 10^{14}\,\mathrm{m}^{-3}$
n_{d0}	$1.2 \times 10^{11}\,\mathrm{m}^{-3}$
T_e	6.0 eV
T_i	0.025 eV
E_{0z}	1.5×10^{3} V/m
Q_{d0}	$-4000e$
U_0	3.8×10^{2} m/s
ν_{in}	$9.5 \times 10^{6}\,\mathrm{s}^{-1}$
ν_{dn}	$39\,\mathrm{s}^{-1}$
$m_d g$	8.60×10^{-13} N
β	$1.83 \times 10^{5}\,Pa^{-1}$

APPENDIX A: PLASMA PARAMETERS USED

Here, we list the plasma parameters used for solving the dispersion relation models discussed in Sec. IV. These parameters are based on the dust acoustic wave experiment by FG.[38]

In this experiment, micron-size dust particles were strongly coupled and the dust particles and ions experienced substantial drag forces on the gas. These conditions are similar to those for microgravity except that the ion flow speed is faster than in microgravity conditions.[90,91] An argon glow discharge plasma was ignited by applying a 13.56 MHz radiofrequency voltage of 85 Vpp to an electrode in a vacuum chamber. Dust particles, which were 4.8 μm melamine formaldehyde polymer spheres, were injected into the plasma. The dust particles became negatively charged by collecting more electrons than ions due to the higher thermal velocity of electrons and were levitated vertically by sheath's electric field. The dust particles were confined horizontally, to form a 3D dust cloud, by placing a glass box above the powered electrode. The dust acoustic wave was self excited with a frequency of 25 Hz at a pressure of 410 mTorr because the energy gained by the ion streaming instability was stronger than the damping due to dust-neutral collisions. The parameters from this experiment that we use in this paper are listed in Table II, based on Table 1 of FG.[38]

Generally, there are two methods of estimating the dust particle charge: a force balance method that equates the gravitational force to the electric force acting on the dust particle or an equating of the OML electron and ion currents onto the dust particle. In FG,[38] the former method was used.

APPENDIX B: DIMENSIONLESS PARAMETERS

Here, we list the dimensionless parameters introduced in Sec. III.

$$\Omega_n = \omega_{pi}\left\{\begin{array}{l} i\dfrac{kU_0}{\omega_{pi}} + D_0 D_3 \dfrac{U_0}{V_{Ti}} + k^2\lambda_{Di}^2 D_2 - iD_1 D_2 D_3 k\lambda_{Di} \\ -\gamma\dfrac{a}{\lambda_{Di}}\dfrac{V_{Ti}}{2U_0} D_3\left(\dfrac{\omega_{pi}}{\Omega_{\phi s} - i\omega}\right)\left(D_0\dfrac{U_0}{V_{Ti}} - iD_1 D_2 k\lambda_{Di}\right) \end{array}\right\}, \tag{B1}$$

$$\Omega_\phi = \omega_{pi}\left\{\begin{array}{l} k^2\lambda_{Di}^2 D_2 - D_0 D_3 D_4 \dfrac{U_0}{V_{Ti}}\dfrac{m_i}{m_d} Z_d k^2 \lambda_{Di}^2 - iD_1 D_2 D_3 k\lambda_{Di} \\ +\gamma D_3 \dfrac{V_{Ti}}{2U_0}\left(\dfrac{\omega_{pi}}{\Omega_{\phi s} - i\omega}\right)\left(2\sqrt{\dfrac{2}{\pi}}\dfrac{\omega_{pe}}{\omega_{pi}}\dfrac{a}{\lambda_{De}}e^{\eta} + iakD_1 D_2\right) \end{array}\right\}, \tag{B2}$$

$$\Omega_{\phi s} = \omega_{pe}\left\{\frac{1}{\sqrt{2\pi}}\frac{a}{\lambda_{De}}e^{\eta} + \gamma\frac{a}{2\lambda_{Di}}\frac{\omega_{pi}}{\omega_{pe}}\frac{V_{Ti}}{U_0}\right\}, \tag{B3}$$

$$\Omega_{V0} = \omega_{pe}\left\{\frac{1}{\sqrt{2\pi}}\frac{a}{\lambda_{De}}e^{\eta} + D_0\frac{aU_0}{4\lambda_{Di}^2\omega_{pe}}\frac{\Omega_\phi}{(\Omega_n - i\omega)} + i\frac{ak}{4}\frac{\omega_{pi}}{\omega_{pe}}D_1 D_2\left(1 - \frac{\Omega_\phi}{(\Omega_n - i\omega)}\right)\right\}. \tag{B4}$$

These expressions use the dimensionless parameters: $\eta = e\phi_s/k_B T_e$, $D_0 = (1 - 2e\phi_s/m_i U_0^2)\gamma$, $D_1 = (1 + 2e\phi_s/m_i U_0^2)\gamma$, $D_2 = \omega_{pi}/[\upsilon_{in} - i(\omega - U_0 k)]$, $D_3 = \pi a^2 \lambda_{Di} n_{d0}$, and $D_4 = \omega_{pi}^2/[\omega^2 - k^2/\beta n_d m_d + i\upsilon_{dn}\omega]$.

Here, $\gamma = I_i/I_{OML}$ is an adjustable dimensionless parameter that allows the use of any ion current model. For the OML ion current model, $\gamma = 1$.

APPENDIX C: RESULTS FOR SENSITIVITY TO EXPERIMENTAL PARAMETERS

Here, we report a sensitivity analysis of the dispersion relation solutions to experimental parameters, such as ambient gas pressure, which do not explicitly appear in our dispersion relations. We compute the exponents for δ_r and δ_i as described in Sec. V A. Results are listed in Table III.

Among the experimental parameters listed in the first column of Table III, most of them only affect one theoretical parameter in the dispersion relations. For example, the ion density n_i only affects the ion plasma frequency ω_{pi}. There are altogether five such parameters: the ion density, electron density, dust density, electron temperature, and ion temperature. The microscopic dc electric field E_z and the ambient gas pressure P, however, affect more than one theoretical parameter in the dispersion relations. In particular, a change in E_z (proportional to U_0 and inversely proportional to Q_d) affects the ion-drift speed and the dust charge due to the levitation requirement, whereas a change in P (proportional to ν_{in}, ν_{dn} and inversely proportional to U_0) affects the ion-neutral collision rate, dust-neutral collision rate, and the ion-drift speed.

As can be seen in the results in Table III, four of the seven parameters have large exponents, i.e., large $|\delta_r|$ or $|\delta_i|$. These four are: ion density, dust density, dc electric field, and gas pressure. Hence, errors in measurements of these parameters can greatly affect theoretical calculation of ω_r and ω_i using the dispersion relations.

TABLE III. Sensitivity of ω_r and ω_i to experimental parameters. The exponents δ_r and δ_i are computed as discussed in Sec. V A. The first column is the parameter F in Eq. (30). Note: an entry of 0.00^* in this table indicates that the magnitude of the exponent is less than 0.01.

	Hydrodynamic models					
	Baseline model		with more processes		Hybrid hydrodynamic-kinetic model	
F	δ_r	δ_i	δ_r	δ_i	δ_r	δ_i
n_i	**−0.47**	−0.16	**−0.44**	+0.09	**−0.46**	−0.12
n_e	$+0.00^*$	−0.06	−0.12	+0.04	$+0.00^*$	−0.07
n_d	**+0.44**	**+2.06**	**+0.61**	**+2.13**	**+0.44**	**+2.08**
T_e	-0.00^*	+0.06	+0.01	+0.08	-0.00^*	+0.07
T_i	-0.00^*	−0.21	-0.00^*	−0.21	+0.01	−0.22
E_z	−0.39	**−3.23**	**−0.73**	**−2.10**	**−0.40**	**−3.32**
P	−0.13	**−3.27**	+0.03	**−4.49**	−0.14	**−3.26**

[1]T. G. Northrop, Phys. Scr. **45**, 475 (1992).
[2]D. A. Mendis and M. Rosenberg, Annu. Rev. Astron. Astrophys. **32**, 419 (1994).
[3]P. K. Shukla, Phys. Plasmas **8**, 1791 (2001).
[4]P. K. Shukla and A. A. Mamun, *Introduction to Dusty Plasma Physics* (Institute of Physics, Bristol, 2002).
[5]A. Piel and A. Melzer, Adv. Space Res. **29**, 1255 (2002).
[6]V. E. Fortov, A. V. Ivlev, S. A. Khrapak, A. G. Khrapak, and G. E. Morfill, Phys. Rep **421**, 1 (2005).
[7]A. Melzer and J. Goree, in *Low Temperature Plasmas*, edited by R. Hippler, H. Kersten, M. Schmidt, and K. H. Schoenbach (Wiley, Weinheim, 2008).
[8]P. K. Shukla and B. Eliasson, Rev. Mod. Phys. **81**, 25 (2009).
[9]G. E. Morfill and A. V. Ivlev, Rev. Mod. Phys. **81**, 1353 (2009).
[10]N. N. Rao, P. K. Shukla, and M. Y. Yu, Planet. Space Sci. **38**, 543 (1990).
[11]A. Barkan, R. L. Merlino, and N. D'Angelo, Phys. Plasmas **2**, 3563 (1995).
[12]H. R. Prabhakara and V. L. Tanna, Phys. Plasmas **3**, 3176 (1996).
[13]C. Thompson, A. Barkan, N. D'Angelo, and R. L. Merlino, Phys. Plasmas **4**, 2331 (1997).
[14]R. L. Merlino, A. Barkan, C. Thompson, and N. D'Angelo, Plasma Phys. Controlled Fusion **39**, A421 (1997); Phys. Plasmas **5**, 1607 (1998).
[15]E. Thomas, Jr. and M. Watson, Phys. Plasmas **6**, 4111 (1999).
[16]V. I. Molotkov, A. P. Nefedov, V. M. Torchinskiĭ, V. E. Fortov, and A. G. Khrapak, J. Exp. Theor. Phys. **89**, 477 (1999).
[17]V. E. Fortov, A. G. Khrapak, S. A. Khrapak, V. I. Molotkov, A. P. Nefedov, O. F. Petrov, and V. M. Torchinsky, Phys. Plasmas **7**, 1374 (2000).
[18]A. A. Samaryan, A. V. Chernyshev, O. F. Petrov, A. P. Nefedov, and V. E. Fortov, J. Exp. Theor. Phys. **92**, 454 (2001).
[19]E. Thomas, Jr. and R. L. Merlino, IEEE Trans. Plasma Sci. **29**, 152 (2001).
[20]N. Hayashi, Phys. Plasmas **8**, 3051 (2001).
[21]A. V. Zobnin, A. D. Usachev, O. F. Petrov, and V. E. Fortov, J. Exp. Theor. Phys. **95**, 429 (2002).
[22]V. E. Fortov, A. D. Usachev, A. V. Zobnin, V. I. Molotkov, and O. F. Petrov, Phys. Plasmas **10**, 1199 (2003).
[23]C. M. Ticoş, A. Dyson, P. W. Smith, and P. K. Shukla, Plasma Phys. Controlled Fusion **46**, B293 (2004).
[24]M. Schwabe, M. Rubin-Zuzic, S. Zhdanov, H. M. Thomas, and G. E. Morfill, Phys. Rev. Lett. **99**, 095002 (2007).
[25]T. Trottenberg, D. Block, and A. Piel, Phys. Plasmas **13**, 042105 (2006).

[26]E. Thomas, Jr., Phys. Plasmas **13**, 042107 (2006).
[27]E. Thomas, Jr., R. Fisher, and R. L. Merlino, Phys. Plasmas **14**, 123701 (2007).
[28]J. D. Williams, E. Thomas, Jr., and L. Marcus, Phys. Plasmas **15**, 043704 (2008).
[29]C.-T. Liao, L.-W. Teng, C.-Y. Tsai, C.-W. Io, and I. Lin, Phys. Rev. Lett. **100**, 185004 (2008).
[30]S.-H. Kim, J. R. Heinrich, and R. L. Merlino, Phys. Plasmas **15**, 090701 (2008).
[31]L.-W. Teng, M.-C. Chang, Y.-P. Tseng, and I. Lin, Phys. Rev. Lett. **103**, 245005 (2009).
[32]J. Heinrich, S.-H. Kim, and R. L. Merlino, Phys. Rev. Lett. **103**, 115002 (2009).
[33]I. Pilch, T. Reichstein, and A. Piel, Phys. Plasmas **16**, 123709 (2009).
[34]J. D. Williams and J. Duff, Phys. Plasmas **17**, 033702 (2010).
[35]J. D. Williams and E. K. Snipes, IEEE Trans. Plasma Sci. **38**, 847 (2010).
[36]R. Fisher and E. Thomas, Jr., IEEE Trans. Plasma Sci. **38**, 833 (2010).
[37]E. Thomas, Jr., Phys. Plasmas **17**, 043701 (2010).
[38]T. M. Flanagan and J. Goree, Phys. Plasmas **17**, 123702 (2010).
[39]T. M. Flanagan and J. Goree, Phys. Plasmas **18**, 013705 (2011).
[40]J. R. Heinrich, S.-H. Kim, J. K. Meyer, and R. L. Merlino, Phys. Plasmas **18**, 113706 (2011).
[41]R. L. Merlino, J. R. Heinrich, S.-H. Kim, and J. K. Meyer, Plasma Phys. Controlled Fusion **54**, 124014 (2012).
[42]J. R. Heinrich, S.-H. Kim, J. K. Meyer, R. L. Merlino, and M. Rosenberg, Phys. Plasmas **19**, 083702 (2012).
[43]W. D. S. Ruhunusiri and J. Goree, Phys. Rev. E **85**, 046401 (2012).
[44]M.-C. Chang, L.-W. Teng, and I. Lin, Phys. Rev. E **85**, 046410 (2012).
[45]Y. -Y Tsai, M.-C. Chang, and I. Lin, Phys. Rev. E **86**, 045402 (2012).
[46]M.-C. Chang, Y.-Y. Tsai, and I. Lin, Phys. Plasmas **20**, 083703 (2013).
[47]A. Piel, M. Klindworth, O. Arp, A. Melzer, and M. Wolter, Phys. Rev. Lett. **97**, 205009 (2006).
[48]A. Piel, O. Arp, M. Klindworth, and A. Melzer, Phys. Rev. E **77**, 026407 (2008).
[49]K. O. Menzel, O. Arp, and A. Piel, Phys. Rev. Lett. **104**, 235002 (2010).
[50]K. O. Menzel, O. Arp, and A. Piel, Phys. Rev. E **83**, 016402 (2011).
[51]M. H. Thoma, H. Höfner, M. Kretschmer, S. Ratynskaia, G. E. Morfill, A. Usachev, A. Zobnin, O. Petrov, and V. Fortov, Microgravity Sci. Technol. **18**, 47 (2006).
[52]F. Melandsø, T. Aslaksen, and O. Havnes, Planet. Space Sci. **41**, 321 (1993).
[53]H. Thomas, G. E. Morfill, V. Demmel, J. Goree, B. Feuerbacher, and D. Möhlmann, Phys. Rev. Lett. **73**, 652 (1994).
[54]M. S. Murillo, Phys. Plasmas **11**, 2964 (2004).
[55]M. Bonitz, C. Henning, and D. Block, Rep. Prog. Phys. **73**, 066501 (2010).
[56]X. Wang, A. Bhattacharjee, and S. Hu, Phys. Rev. Lett. **86**, 2569 (2001).
[57]G. Piacente, F. M. Peeters, and J. J. Betouras, Phys. Rev. E **70**, 036406 (2004).
[58]G. Uchida, U. Konopka, and G. Morfill, Phys. Rev. Lett **93**, 155002 (2004).
[59]X.-F. Yang, Y. Liu, J. Cui, and Y. Zhang, Phys. Plasmas **19**, 073709 (2012).
[60]N. D'Angelo and R. L. Merlino, Planet. Space Sci. **44**, 1593 (1996).
[61]N. D'Angelo, Phys. Plasmas **4**, 3422 (1997).
[62]M. Rosenberg, Planet. Space Sci. **41**, 229 (1993).
[63]M. Rosenberg, J. Vac. Sci. Technol. A **14**, 631 (1996).
[64]M. Rosenberg and G. Kalman, Phys. Rev. E **56**, 7166 (1997).
[65]P. K. Kaw and A. Sen, Phys. Plasmas **5**, 3552 (1998).
[66]M. S. Murillo, Phys. Plasmas **5**, 3116 (1998).
[67]P. K. Shukla, G. T. Birk, and G. Morfill, Phys. Scr. **56**, 299 (1997).
[68]N. D'Angelo, Phys. Plasmas **5**, 3155 (1998).
[69]A. A. Mamun and P. K. Shukla, Phys. Plasmas **7**, 4412 (2000).
[70]B. S. Xie and M. Y. Yu, Phys. Rev. E **62**, 8501 (2000).
[71]P. K. Shukla and D. Resendes, Phys. Plasmas **7**, 1614 (2000).
[72]K. N. Ostrikov, S. V. Vladimirov, M. Y. Yu, and G. E. Morfill, Phys. Rev. E **61**, 4315 (2000).
[73]S. V. Annibaldi, A. V. Ivlev, U. Konopka, S. Ratynskaia, H. M. Thomas, G. E. Morfill, A. M. Lipaev, V. I. Molotkov, O. F. Petrov, and V. E. Fortov, New J. Phys. **9**, 327 (2007).
[74]R. L. Merlino, Phys. Plasmas **16**, 124501 (2009).
[75]V. V. Yaroshenko, V. Nosenko, and G. E. Morfill, Phys. Plasmas **17**, 103709 (2010).
[76]V. V. Yaroshenko, S. A. Khrapak, H. M. Thomas, and G. E. Morfill, Phys. Plasmas **19**, 023702 (2012).
[77]V. V. Yaroshenko, S. A. Khrapak, H. M. Thomas, and G. E. Morfill, IEEE Trans. Plasma Sci. **41**, 2446 (2013).
[78]C. K. Goertz, Rev. Geophys. **27**, 271, doi:10.1029/RG027i002p00271 (1989).
[79]O. Havnes, T. K. Aanesen, and F. Melandsø, J. Geophys. Res. **95**, 6581 (1990).
[80]J. Goree, Plasma Sources Sci. Technol. **3**, 400 (1994).
[81]R. L. Merlino and J. Goree, Phys. Today **57**(7), 32 (2004).
[82]H. Ikezi, Phys. Fluids **29**, 1764 (1986).
[83]S. Ichimaru, H. Iyetomi, and S. Tanaka, Phys. Rep. **149**, 91 (1987).
[84]P. M. Bellan, *Fundamentals of Plasma Physics*, 1st ed. (Cambridge University Press, Cambridge, 2006).
[85]E. C. Whipple, Rep. Prog. Phys. **44**, 1197 (1981).
[86]M. Lampe, R. Goswami, Z. Sternovsky, S. Robertson, V. Gavrishchaka, G. Ganguli, and G. Joyce, Phys. Plasmas **10**, 1500 (2003).
[87]S. A. Khrapak, S. V. Ratynskaia, A. V. Zobnin, A. D. Usachev, V. V. Yaroshenko, M. H. Thoma, M. Kretshcmer, H. Höfner, G. E. Morfill, O. F. Petrov, and V. E. Fortov, Phys. Rev. E **72**, 016406 (2005).
[88]See supplementary material at http://dx.doi.org/10.1063/1.4879816 for derivations of Eqs. (14) and (25).
[89]D. A. Gurnett and A. Bhattacharjee, *Introduction to Plasma Physics: With Space and Laboratory Applications*, 1st ed. (Cambridge University Press, Cambridge, 2005).
[90]M. Rosenberg, G. J. Kalman, P. Hartmann, and J. Goree, Phys. Rev. E **89**, 013103 (2014).
[91]O. Arp, J. Goree, and A. Piel, Phys. Rev. E **85**, 046409 (2012).